JOURNAL OF COMPUTATIONAL PHYSICS **143,** 426–448 (1998)
ARTICLE NO. CP985984

On the Finite Difference-Based Lattice Boltzmann Method in Curvilinear Coordinates

Renwei Mei and Wei Shyy

Department of Aerospace Engineering, Mechanics & Engineering Science, University of Florida, Gainesville, Florida 32611-6250

Received August 26, 1997; revised February 26, 1998

The lattice Boltzmann method is a microscopic-based approach for solving the fluid flow problems at the macroscopic scales. The presently popular method uses regularly spaced lattices and cannot handle curved boundaries with desirable flexibility. To circumvent such difficulties, a finite difference-based lattice Boltzmann method (FDLBM) in curvilinear coordinates is explored using body-fitted coordinates with non-uniform grids. Several test cases, including the impulsively started cylindrical Couette flow, steady state cylindrical Couette flow, steady flow over flat plates, and steady flow over a circular cylinder, are used to examine various issues related to the FDLBM. The effect of boundary conditions for the distribution functions on the solution, the merits between second-order central difference and upwind schemes for advection terms, and the effect of the Reynolds number are investigated. Favorable results are obtained using FDLBM in curvilinear coordinates, indicating that the method is potentially capable of solving finite Reynolds number flow problems in complex geometries.

1. INTRODUCTION

There has been rapid development of the Lattice Boltzmann method (LBM) as an alternative numerical method for simulating fluid dynamics problems [4]. In traditional numerical methods, the macroscopic variables, such as velocity and density, are obtained by solving the Navier–Stokes (NS) equations. The LBM solves the microscopic kinetic equation for particle distribution function f_i from which the macroscopic quantities (velocity and density) are obtained through moment integration of f_i. In the kinetic equation for f_i (see Eq. (1)), the advection operator is linear in the phase space while the convection term is non-linear in the NS equations. A BGK type simple relaxation process in the kinetic equation allows the recovery of the non-linear convection in the NS equations through the multi-scale expansion. In the nearly incompressible flow limit, the NS equations are recovered. In particular, the pressure is typically obtained by solving the Poisson equation (or an equivalent one)

0021-9991/98 $25.00

derived from the incompressible NS equations which can be time consuming. In LBM, the pressure is obtained through an extremely simple equation of state [6], $p = \rho c_s^2$, in which ρ is the fluid density and c_s is the speed of sound. This is a quite appealing feature of the LBM. The discretized equation for f_i is explicit and easy to implement in parallel processing. At low Reynolds number, LBM can handle very complex geometry such as multiphase flow in porous media or through small holes [4].

The Boltzmann equation governing the velocity distribution function $f(t, \mathbf{c}, \mathbf{x})$ may be written, with a single relaxation time τ, as

$$\frac{\partial f}{\partial t} + \mathbf{c} \cdot \nabla f = -\frac{1}{\tau}(f - f^{eq}), \tag{1a}$$

where f^{eq} is the equilibrium distribution. After discretizing the velocity space $\mathbf{c}$ into various directions, the Boltzmann equation for the velocity distribution function f_i may be written as

$$\frac{\partial f_i}{\partial t} + \mathbf{c}_i \cdot \nabla f_i = -\frac{1}{\tau}\left(f_i - f_i^{eq}\right) \qquad (i = 0, 1, \ldots, 8 \quad \text{for 2-D}) \tag{1b}$$

[1, 3, 8] where f_i^{eq} is the equilibrium distribution of f_i chosen to satisfy the NS equation and $\mathbf{c}_i$ is the lattice velocity in the ith-direction. In a 2-D, 9-speed square lattice,

$$\mathbf{c}_i = (\cos((i-1)\pi/4),\ \sin((i-1)\pi/4)) \qquad \text{for } i = 1, 3, 5, 7,$$
$$\mathbf{c}_i = \sqrt{2}(\cos((i-1)\pi/4),\ \sin((i-1)\pi/4)) \qquad \text{for } i = 2, 4, 6, 8, \quad \text{and} \quad \mathbf{c}_0 = 0.$$

It is noted that Eq. (1b) is one of numerous possible ways to model the transport of f_i. The density ρ and momentum flux $\rho\mathbf{u}$ are obtained from

$$\rho = \sum_i f_i \qquad \text{and} \qquad \rho\mathbf{u} = \sum_i \mathbf{c}_i f_i. \tag{2}$$

In a 9-speed square lattice, a suitable equilibrium distribution function often takes the form [4, 8]

$$f_i^{eq} = \rho\alpha_i\left[1 + 3\mathbf{c}_i \cdot \mathbf{u} + \frac{9}{2}(\mathbf{c}_i \cdot \mathbf{u})^2 - \frac{3}{2}u^2\right] \tag{3}$$

with $\alpha_0 = 4/9$, $\alpha_1 = \alpha_3 = \alpha_5 = \alpha_7 = 1/9$, and $\alpha_2 = \alpha_4 = \alpha_6 = \alpha_8 = 1/36$. This gives the speed of sound $c_s = \sqrt{1/3}$ in a lattice unit. If Eq. (1b) is solved exactly using f_i^{eq} given by Eq. (3), the viscosity of the fluid is $\nu = \tau/3$ [1, 8]. In the classical BGK model, Eq. (1b) is solved in the form of

$$f_i(\mathbf{x} + \mathbf{c}_i, t + 1) - f_i(\mathbf{x}, t) = -\frac{1}{\tau}\left(f_i(\mathbf{x}, t) - f_i^{eq}(\mathbf{x}, t)\right) \tag{4}$$

using $\Delta x = \Delta y = \Delta t = 1$. The discretized equation (4) recovers the NS equations in the nearly incompressible flow limit. Because f_i^{eq} in (3) is derived based on Talor series expansion for small velocity, it is desirable that the maximum flow speed does not exceed 20% of c_s. Equation (4) can be viewed as a specially discretized form of Eq. (1b) in which the advection term $\mathbf{c}_i \cdot \nabla f_i$ is evaluated using a first order down-wind difference. The negative

numerical diffusion introduced by the use of the first order down-wind difference can be exactly accounted for by modifying the viscosity from $\tau/3$ to $\tau/3 - 1/6$ with a second order accuracy in both space and time [6]. Depending on the treatment of the boundary conditions [5] for f_i, τ may not be very close to $1/2$ for stability reasons. This implies that a practical lower limit on ν may be imposed and flows with high Reynolds number have been typically simulated using a large number of uniform lattices to give a large value of the characteristic length of the domain.

The use of $\Delta x = \Delta y = \Delta t = 1$ is quite restrictive in many applications involving external flows where a large gradient exists only in a small region while the domain of interest is large. It has been demonstrated that Eq. (1b) can be solved using non-uniform grids [9]. Successful implementation was carried out for flow in a channel with a sudden expansion and flow over a cylinder using an interpolation procedure [10]. Cao *et al.* [3] have shown that Eq. (1b) can be viewed as a transport equation for f_i and can be solved using a finite difference method. Central differencing was used for ∇f_i in several examples with simple geometries. In this approach, smaller viscosity ν $(=\tau/3)$ can be used since Δt can now be chosen independent of Δx. This allows for simulations at higher Reynolds numbers or for flows with rapid transient features.

High Reynolds number flows around non-Cartesian objects are often of interest to a large class of engineering problems. At finite *Re*, the integrity of geometry is extremely important. Although LBM based on the BGK model in Cartesian coordinates has been shown to be effective to obtain the overall force on moving objects at low Reynolds number, it is not the case at high *Re* since the vorticity generation is sensitive to the geometrical resolution. The absence of using body fitted coordinates in LBM primarily results from the restriction of the lattice BGK (LBGK) equation to the rectangle lattice/grid and from difficulties in implementing boundary conditions for f_i on a solid wall. As Succi [20] pointed out, "to the best of the authors knowledge, to date, nobody knows how to extend synchronous LBE schemes ... to generalized coordinates and/or irregular mesh distributions. This is a major stumbling block, as it rules out a host of important real-life engineering applications." He also observed that "the problem has been (partially) circumvented by marrying LBE with standard finite-volume and, more recently, finite-difference technique. By adopting a generic time-marching and space-discretization scheme, the synchronization between discrete speeds and the spatial stencil is generally spoiled. This is precisely where the geometrical flexibility comes from, since the spatial stencil is now set free from the symmetry requirements imposed to the discrete speeds. The price for geometrical freedom is the need to interpolate between the particle positions generated by the discrete speeds and the sites of the spatial grids." While LBM appears to have potential to compete with or surpass the standard finite difference/finite volume/finite element methods for solving the NS equations at high Reynolds numbers, clearly many fundamental and practical issues need to be systematically addressed.

In this paper, the finite difference based lattice Boltzmann method (FDLBM) of Cao *et al.* [3] is extended to curvilinear coordinates with non-uniform grids. In body-fitted coordinates, the geometry of the solid boundaries can often be more easily preserved. In the present effort, boundary conditions for the f_i's are examined, and the impacts of discretizing the convection term, $\mathbf{c}_i \cdot \nabla f_i$, using central difference and second order upwind schemes on the behavior of the solution are assessed. Several flows are solved using FDLBM, including impulsively started cylindrical Couette flow, steady state cylindrical Couette flow, steady flow over flat plates, and steady flow over a circular cylinder. The primary focus of the

paper is to assess the accuracy of the solution based on FDLBM at finite Reynolds number. Pertinent comparisons are made with the LBGK solutions and finite difference solutions for the NS equations.

2. FORMULATIONS

2.1. *Transformed Equations in Curvilinear Coordinates*

To preserve the geometry of the curved boundary, Eq. (1b) can be solved in a body-fitted curvilinear coordinate system (Fig. 1) using the finite difference method. Let $\mathbf{r} = (x, y, z)$ be transformed to a curvilinear coordinate (ξ_1, ξ_2, ξ_3) so that Eq. (1) becomes

$$\frac{\partial f_i}{\partial t} + \frac{1}{\sqrt{g}}\mathbf{c}_i \cdot \sum_{m=1}^{3}(\mathbf{a}_j \times \mathbf{a}_k)\frac{\partial f_i}{\partial \xi_m} = -\frac{1}{\tau}\left(f_i - f_i^{eq}\right), \tag{5}$$

where

$$\mathbf{a}_j = \frac{\partial \mathbf{r}}{\partial \xi_j}, \qquad \text{and} \qquad \sqrt{g} = \det|g_{jk}| = \mathbf{a}_1 \cdot (\mathbf{a}_2 \times \mathbf{a}_3). \tag{6}$$

The grid system can be generated numerically with desirable distributions. The dependent variables, f_i, do not change with the choice of coordinate systems. Equation (5) can be discretized using the finite difference and the resulting equation is solved in an explicit manner. Since $\mathbf{c}_i$ is defined in the Cartesian coordinates and f_i is a scalar, the Cartesian velocity (u, v, w) and density ρ can be easily obtained using Eq. (2) in the curvilinear coordinate system. Due to the absence of the second order spatial derivatives, the transport equations for f_i's are simpler than the transformed NS equations in curvilinear coordinates.

Throughout the rest of this paper, only 2-D problems will be considered for simplicity. In polar coordinates (r, θ), Eq. (5) becomes

$$\frac{\partial f_i}{\partial t} + c_{i\theta}\frac{1}{r}\frac{\partial f_i}{\partial \theta} + c_{ir}\frac{\partial f_i}{\partial r} = -\frac{1}{\tau}\left(f_i - f_i^{eq}\right), \tag{7}$$

where

$$c_{ir} = c_{ix}\cos(\theta) + c_{iy}\sin(\theta), \tag{8a}$$

$$c_{i\theta} = -c_{ix}\sin(\theta) + c_{iy}\cos(\theta). \tag{8b}$$

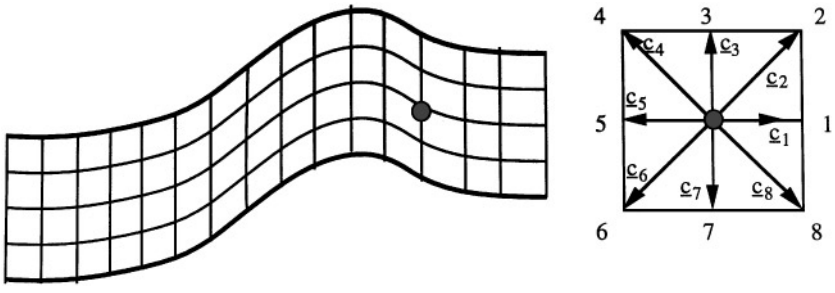

FIG. 1. Grids in a body fitted curvilinear coordinate and a 2-D 9-bit lattice.

If a one-dimensional grid stretching in the r-direction is applied, $r = r(\eta)$, the above becomes

$$\frac{\partial f_i}{\partial t} + \frac{1}{r} c_{i\theta} \frac{\partial f_i}{\partial \theta} + \frac{c_{ir}}{h_r} \frac{\partial f_i}{\partial \eta} = -\frac{1}{\tau}\left(f_i - f_i^{eq}\right), \tag{9}$$

where

$$h_r = \frac{dr}{d\eta}. \tag{10}$$

In Cartesian coordinates, after one-dimensional stretching $x = x(\xi)$ and $y = y(\eta)$ are applied, Eq. (5) becomes

$$\frac{\partial f_i}{\partial t} + \frac{c_{ix}}{h_x} \frac{\partial f_i}{\partial \xi} + \frac{c_{iy}}{h_y} \frac{\partial f_i}{\partial \eta} = -\frac{1}{\tau}\left(f_i - f_i^{eq}\right), \tag{11}$$

where $h_x = dx/d\xi$ and $h_y = dy/d\eta$.

2.2. *Discretization of the Transformed Equations*

Equation (9), or (11), is a transport equation for f_i with order one advection velocity c_i but does not possess an explicit diffusion. When a central difference approximation is applied, $\partial f_i/\partial \xi$ is

$$\left.\frac{\partial f_i}{\partial \xi}\right|_{centr} = \frac{f_i(jx+1, jy) - f_i(jx-1, jy)}{2\Delta\xi} \tag{12}$$

at grid point (jx, jy) regardless of the direction of the particle velocity c_i. For convection dominated physical problems, it is known that such a central difference approximation for the convection term may lead to artificial wiggles in the solution. However, a first order upwind difference for the convection term will often lead to strong numerical dissipation for finite Reynolds number flows which can significantly change the physics of the flow. A popular approach is to adopt the higher order upwind discretization scheme. For the Boltzmann equation, (9) or (11), the situation is more severe since c_{ix} or c_{iy} is still an order one quantity on the solid wall, although the fluid velocity $\mathbf{u}$ may be zero. To maintain desirable accuracy, one can employ the second order upwind difference scheme [18]. In Eq. (9), for example, $\partial f_i/\partial \xi$ can be approximated as

$$\begin{aligned}\left.\frac{\partial f_i}{\partial \xi}\right|_{2up} &= \frac{3f_i(jx, jy) - 4f_i(jx-1, jy) + f_i(jx-2, jy)}{2\Delta\xi} \qquad \text{if } c_{i\theta} \geq 0 \\ &= \frac{-3f_i(jx, jy) + 4f_i(jx+1, jy) - f_i(jx+2, jy)}{2\Delta\xi} \qquad \text{if } c_{i\theta} < 0,\end{aligned} \tag{13}$$

where jx and jy are the grid number in ξ- and η-directions, respectively.

It should be pointed out that the interpolation supplemented LBM [9] and the present finite difference based LBM are two methods solving Boltzmann equation in curvilinear coordinates. These two methods are in fact close in spirit. The first one starts directly from the LBGK form which is a special finite difference discretization of the Boltzmann equation. Their approach is a Lagrangian one, similar to a Riemann solver in which one tracks the

advancement of a moving signal, then reconstructs the signal (distribution function f_i) at field locations by an interpolation procedure. The current FDLBM, on the other hand, considers the movement of the signal, f_i, in an Eulerian sense. Hence we transform the coordinates so that the lattice vertices and the signal locations are evaluated based on the flux estimation. In the present FDLBM, the "second order upwind" is naturally embedded in the solution. In the interpolation supplemented LBM, a second-order upwind type of interpolation was also used to maintain the correct signal propagation.

In order to simulate higher Reynolds number flows, it is desirable to use a smaller relaxation time τ. However, when a very small τ is used, Eq. (9) or (11) clearly becomes a stiff equation and is more difficult to solve in an explicit procedure. This issue does not arise in LBGK since $\tau > 1/2$ is already imposed to maintain a positive viscosity so that the explicit treatment of the relaxation term does not violate the stability requirement, $\Delta t/\tau < 2$, for an explicit solver for an ordinary differential equation. An implicit representation for the relaxation term on the right hand side of (9) or (11) is thus preferable in order to use smaller τ and larger Δt. However, the relaxation term is nonlinear in macroscopic variables as f_i^{eq} depends on the products such as ρu and ρu^2. Denoting n as the nth time step on which the solution or initial condition is known, this can be accomplished, without resorting to an iterative procedure, as

$$-\frac{1}{\tau}\left(f_i - f_i^{eq}\right)\Big|^{n+1} = -\frac{1}{\tau}\left[f_i^{n+1} - \left(2f_i^{eq,n} - f_i^{eq,n-1}\right)\right]. \tag{14}$$

The extrapolation for f_i^{eq} ensures that the relaxation term is at the $(n+1)$st time step. Finally, the discretized form of Eq. (9) can be cast in the form of

$$\frac{f_i^{n+1} - f_i^n}{\Delta t} + \frac{1}{r}c_{i\theta}\frac{\partial f_i^n}{\partial \theta}\bigg|_{2up} + \frac{1}{h_r}c_{ir}\frac{\partial f_i^n}{\partial \eta}\bigg|_{2up} = -\frac{1}{\tau}\left[f_i^{n+1} - \left(2f_i^{eq,n} - f_i^{eq,n-1}\right)\right]. \tag{15}$$

Because of the implicit nature of the relaxation term, the stability restriction now mainly results from the explicit treatment of the advection terms which is known as the CFL condition. In principle, since $|\mathbf{c}_i| = 1$, the time step should not exceed the smallest spatial grid size in either direction. In practice, however, the extrapolation for the non-linear relaxation term may contribute to instability if there is a large gradient of the density near a sharp corner. It is worth pointing out that the effect of the extrapolation for $f_i^{eq,n+1}$ has no effect on the viscosity. For an impulsively started Couette flow, the evolution of the velocity distribution depends explicitly on the viscosity. Excellent agreement between the exact solution based on $\nu = \tau/3$ and the FDLBM solution shows that the extrapolation for $f_i^{eq,n+1}$ is appropriate.

In Eq. (15), $(\partial f_i^n/\partial\theta)|_{2up}$ can be replaced by $(\partial f_i^n/\partial\theta)|_{centr}$ as long as no wiggle is detected in the solution. This feature is useful since the central difference is easier to implement and computationally more efficient.

2.3. *Boundary Conditions on a Solid Wall*

There have been several recent studies [5, 16] on the implementation of boundary conditions in the context of (4). A conventional bounce back scheme [11, 12] has been shown to work reliably in conjunction with Eq. (4).

As pointed out in Chen *et al.* [5], if the wall is on the cell of the lattice, the values of f_i's on an interior grid are needed during the streaming portion of the advection step. Physically,

only the fluid velocity $\mathbf{u}$ is usually known on a solid wall. The question remains as to the appropriate strategy for the boundary conditions of f_i when a solid wall is encountered.

Consider a wall at $\eta = 0$ (with $jy = 2$) and the fluid is on the $\eta > 0$ side ($jy > 2$). One should note that the values of $f_i^n(ix, 2)$ on the wall are part of the solution and the physical boundary condition, $\mathbf{u}(ix, 2) = \mathbf{u}_{wall}$, is reflected in the definition of f_i^{eq} (see Eq. (4)). It is proposed that a one-sided difference be used for $\partial f_i/\partial\eta$ on the wall to ease the numerical implementation,

$$\frac{\partial f_i^n}{\partial \eta} = \frac{f_i^n(jx, 3) - f_i^n(jx, 2)}{\Delta\eta}. \tag{16}$$

Equivalently, an artificial grid can be introduced at $\eta = -\Delta\eta$ ($jy = 1$) and the values of f_i at $\eta = -\Delta\eta$ can be obtained using a linear extrapolation [5] as

$$f_i^n(jx, 1) = 2 f_i^n(jx, 2) - f_i^n(jx, 3). \tag{17}$$

The central difference approximation for $\partial f_i^n/\partial\eta$ gives

$$\left.\frac{\partial f_i^n}{\partial \eta}\right|_{centr} = \frac{f_i^n(jx, 3) - f_i^n(jx, 1)}{2\Delta\eta} = \frac{f_i^n(jx, 3) - f_i^n(jx, 2)}{\Delta\eta} \tag{18}$$

which is identical to the one-sided difference given by Eq. (16). Several numerical examples presented below will show that such a treatment on the wall is adequate.

Computational boundary conditions for f_i are very important issues in LBM. Treatments on other kinds of boundaries (such as truncated infinity, symmetry line, and periodic geometry) will be detailed in considering specific numerical examples.

3. NUMERICAL EXAMPLES

The FDLBM outlined above is now applied to solve several simple, yet nontrivial, problems. They are the impulsively started cylindrical Couette flow, the steady state cylindrical Couette flow, a steady flow over a periodic stack of flat plates of finite length and zero thickness, and a steady flow over a circular cylinder. The impulsively started cylindrical Couette flow has a thin Stokes layer at small time which requires a grid stretching in order to adequately resolve the flow field. The steady state cylindrical Couette flow allows the examination of the long-time behavior of the FDLBM. The flow over flat plates encounters singularities in the leading edge and trailing edge where the vorticity or pressure is theoretically singular. The steady flow over a circular cylinder is the most difficult one considered here, as will become clear later, due to possibly the interaction of the numerical boundary condition at infinity with the flow in the wake region.

3.1. *The Impulsively Started Cylindrical Couette Flow*

The unsteady flow between cylinders of radius r_1 and r_2 ($>r_1$) is considered. At $t < 0$, the fluid is at rest. The outer cylinder is started with a velocity U impulsively. Although the tangential velocity is uniform in the θ-direction, the Cartesian components of the velocity, (u_x, u_y), and the velocity distribution functions f_i are not uniform in θ. To implement the exact boundary condition in the θ-direction, the f_i's from $\theta = 0$ to $\theta = 2\pi - \Delta\theta$ are solved

in which $\Delta\theta$ is the step size in the θ-direction. The results for f_i ($i = 0$ to 8), ρ, u_x, and u_y at $\theta = 2\pi$ are set to those at $\theta = 0$ due to periodicity. The periodic condition is also used in evaluating $\partial f_i^n/\partial\theta$ near $\theta = 0$ at every time step. To resolve the thin unsteady Stokes layer, the following stretching is applied in the radial direction

$$r = r_1 + (r_2 - r_1)\frac{1}{\beta}\tan^{-1}[\eta\tan(\beta)], \tag{19}$$

where the parameter $\beta < \pi/2$ controls stretching. A uniform grid distribution can be recovered by using small values of β. A value close to $\pi/2$ results in clustering of the grid near $r = r_2$ or $\eta = 1$.

In the simulation for impulsive starting, the following physical parameters are used: $r_1 = 32$, $r_2 = 64$, $\tau = 0.25$ ($\nu = 0.08333$), and $Re = U(r_2 - r_1)/\nu = 10$. This gives $U = 0.0264$ which is quite small compared with the speed of sound $c_s = 0.577$. Thirty-two intervals are used in the r- and θ-directions, respectively. The stretching parameter is $\beta = 1.0$ and $\Delta t = 0.1$. By increasing the grid resolution in the θ-direction to 64 intervals while keeping the rest of the parameters unchanged, nearly the same velocity profiles are obtained for the initial period considered ($t < 100$ in lattice unit). Both 2nd order upwind difference and central difference for the advection terms are implemented and the results will be compared. Figure 2 shows the tangential velocity variation along the radial direction at $t = 10$, 20, 40, and 100 based on the 2nd order upwind for $\mathbf{c}_i \cdot \nabla f_i$, the central difference for $\mathbf{c}_i \cdot \nabla f_i$, and a finite difference solution for the NS equations in polar

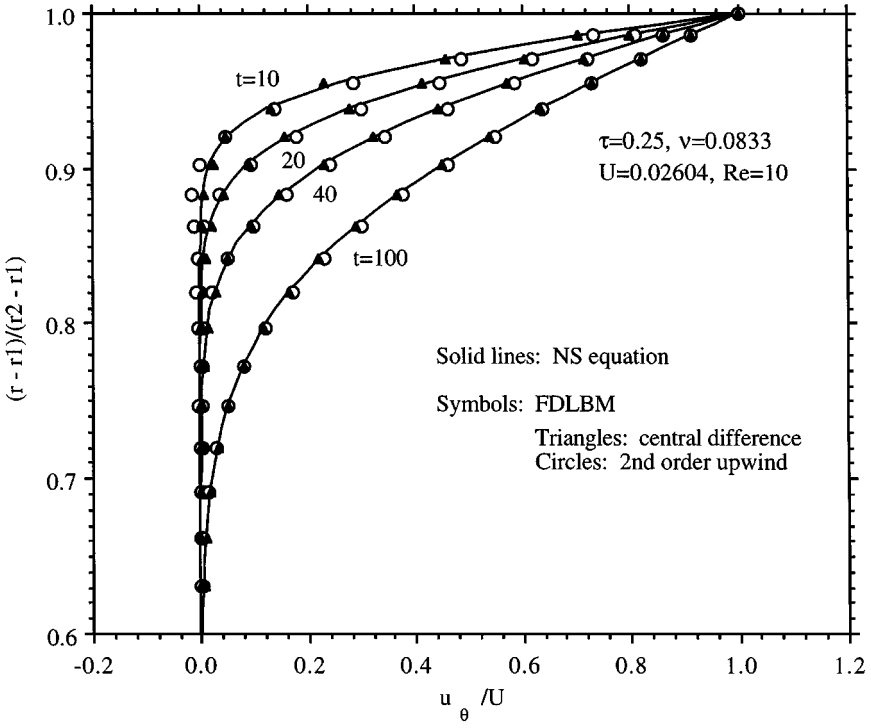

FIG. 2. Comparison of tangential velocity profiles in the impulsively started Couette flow. The NS equation for u_θ is solved using the implicit finite difference scheme with twice the grids in the r-direction used by FDLBM.

coordinates, $\partial u_\theta/\partial t = \nu[(1/r)(\partial/\partial r)(r(\partial u_\theta/\partial r)) - u_\theta/r^2]$, with twice more grid points along the r-direction and the same stretching function given by Eq. (19). The solution to NS equation is intended to serve as an "exact solution." Smaller grid size is used to reduce numerical error in the "exact solution." These instants correspond to dimensionless times based on a diffusion time scale: $t^* = t\nu/(r_2 - r_1)^2 = 8.1438 \times 10^{-4}$, 1.6276×10^{-3}, 3.2552×10^{-3}, and 8.1438×10^{-3}. Except for $t = 10$, three solutions agree very well. For $t = 10$, which is still a very small time, the 2nd order upwind solution has a slight overshoot while the central difference-based solution does not exhibit such an overshoot. However, this slight overshoot can be easily reduced by using $\beta = 1.25$ and $\Delta t = 0.05$. With $\beta = 1.25$, the grid size in r-direction is further reduced so that the numerical error associated with the 2nd order upwind difference is reduced near $r = r_2$ where rapid variations of f_i occur. In Cao *et al.* [3], a predictor-corrector procedure was used to solve for f_i and the relaxation term was kept in an explicit form. In the present formulation, only one step is needed at each time step. It is worth noting that the temporal accuracy of the solution is quite satisfactory despite the use of the first order difference in time. However, if f_i^{eq} in Eq. (15) was not extrapolated to the $(n+1)$ instant while f_i^{n+1} was used in the relaxation term, a noticeable discrepancy in the velocity profile occurs in comparing with the solution of the NS equations due to the mismatch in the collision mechanism represented by the relaxation.

3.2. *Steady State Cylindrical Couette Flow*

For steady state cylindrical Couette flow with the outer cylinder moving at a speed of U, a simple expression for the exact solution of the tangential velocity exists:

$$u_\theta/U = \left(\frac{r_2}{r_1} - \frac{r_1}{r_2}\right)^{-1}\left(\frac{r}{r_1} - \frac{r_1}{r}\right). \tag{20}$$

From the radial component of the NS equations, the pressure variation along r can be obtained as

$$p(r) - p(r_1) = \rho U^2\left(\frac{r_2}{r_1} - \frac{r_1}{r_2}\right)^{-2}\left[\frac{1}{2}\left(\frac{r}{r_1}\right)^2 - 2\log\left(\frac{r}{r_1}\right) - \frac{1}{2}\left(\frac{r_1}{r}\right)^2\right] \tag{21}$$

which is due to the centrifugal force. Since the fluid is nearly incompressible, the density factor in Eq. (21) can take an average value $\bar{\rho}$ as a first approximation and the actual density variation can be obtained from the equation of state in differential from, $dp = c_s^2 d\rho$, as

$$\rho(r) - \rho(r_1) \sim \frac{1}{c_s^2}\bar{\rho}U^2\left(\frac{r_2}{r_1} - \frac{r_1}{r_2}\right)^{-2}\left[\frac{1}{2}\left(\frac{r}{r_1}\right)^2 - 2\log\left(\frac{r}{r_1}\right) - \frac{1}{2}\left(\frac{r_1}{r}\right)^2\right]. \tag{22}$$

In the FDLBM computation, $\beta = 0.2$ is used so that the grid is nearly uniform. The computation starts from a linear velocity profile for u_θ and constant density ρ ($=1.2$) everywhere. The discretized equation used is in the form of Eq. (15). The central difference approximation for $\partial f_i^n/\partial\theta$ and $\partial f_i^n/\partial\eta$ is also implemented to assess the performance of such discretization.

Figure 3 compares the steady state velocity profiles in cylindrical Couette flow between the exact solution given by Eq. (20) and the FDLBM solution based on the central difference scheme using 32 intervals in the r-direction, and 32, 64, and 128 intervals in the θ-direction,

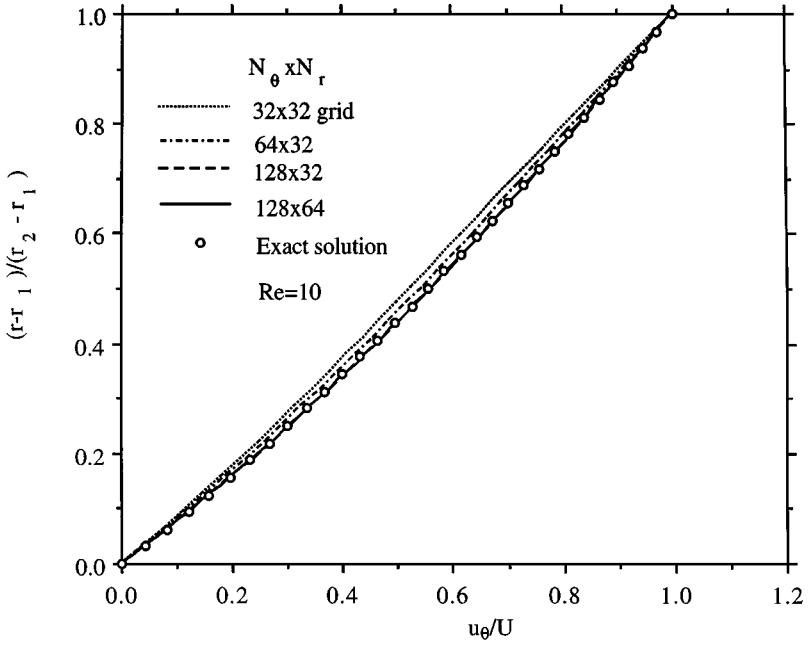

FIG. 3. Comparison of steady state velocity profiles in cylindrical Couette flow between the exact solution and the FDLBM solution based on the central difference formulation. The results based on 2nd order upwind formulation are indistinguishable from that of the central difference. The grid is nearly uniformly distributed in polar coordinates.

respectively. The results based on the 2nd order upwind formulation are indistinguishable from those of the central difference. As the resolution increases in the θ-direction, the steady state solution becomes closer to the exact solution. The results using 64 intervals in the r-direction and 128 intervals in the θ-direction, however, are nearly identical which suggests that 32 intervals are sufficient in the r-direction.

Comparing Fig. 2 with Fig. 3, it is worth noting that in the initial stage of the impulsive starting case, a large gradient occurs in the radial direction so that 32 intervals in the θ-direction are adequate. In the steady state, the resolution in the θ-direction becomes as important as in the r-direction since the variation of f_i in θ is as significant as in r.

Figure 4(a) shows the variations of steady state tangential velocity along the θ-direction in cylindrical Couette flow at a given radial position close to the outer wall, $y = (r - r_1)/(r_2 - r_1) = 0.9084$. Both the 2nd order upwind and the central difference schemes have small amplitude fluctuations. While the amplitudes in both cases are small compared with the mean value, the central difference scheme has a larger fluctuating amplitude and smaller wavelength (on the grid size scale) compared with that based on the 2nd order upwind scheme. Figure 4(b) shows the variations of steady state density along θ at $y = 0.9084$. Again, the central difference based solution has a larger amplitude oscillation and the wavelength of the oscillation is on the grid scale. Figure 4(c) shows the variations of steady state density, $\rho(r) - \rho(r_1)$, along the r-direction. The reference density is taken from $r = r_1$. The analytical solution for $\rho(r) - \rho(r_1)$ is given by Eq. (22). For the central difference based solution, a large grid-scale oscillation in the r-direction is observed. Hence, the reference density is taken from the average value at $r = r_1$ and the first grid away from the inner wall. Noticing that the density variation based on the 2nd order upwind scheme agrees quite well

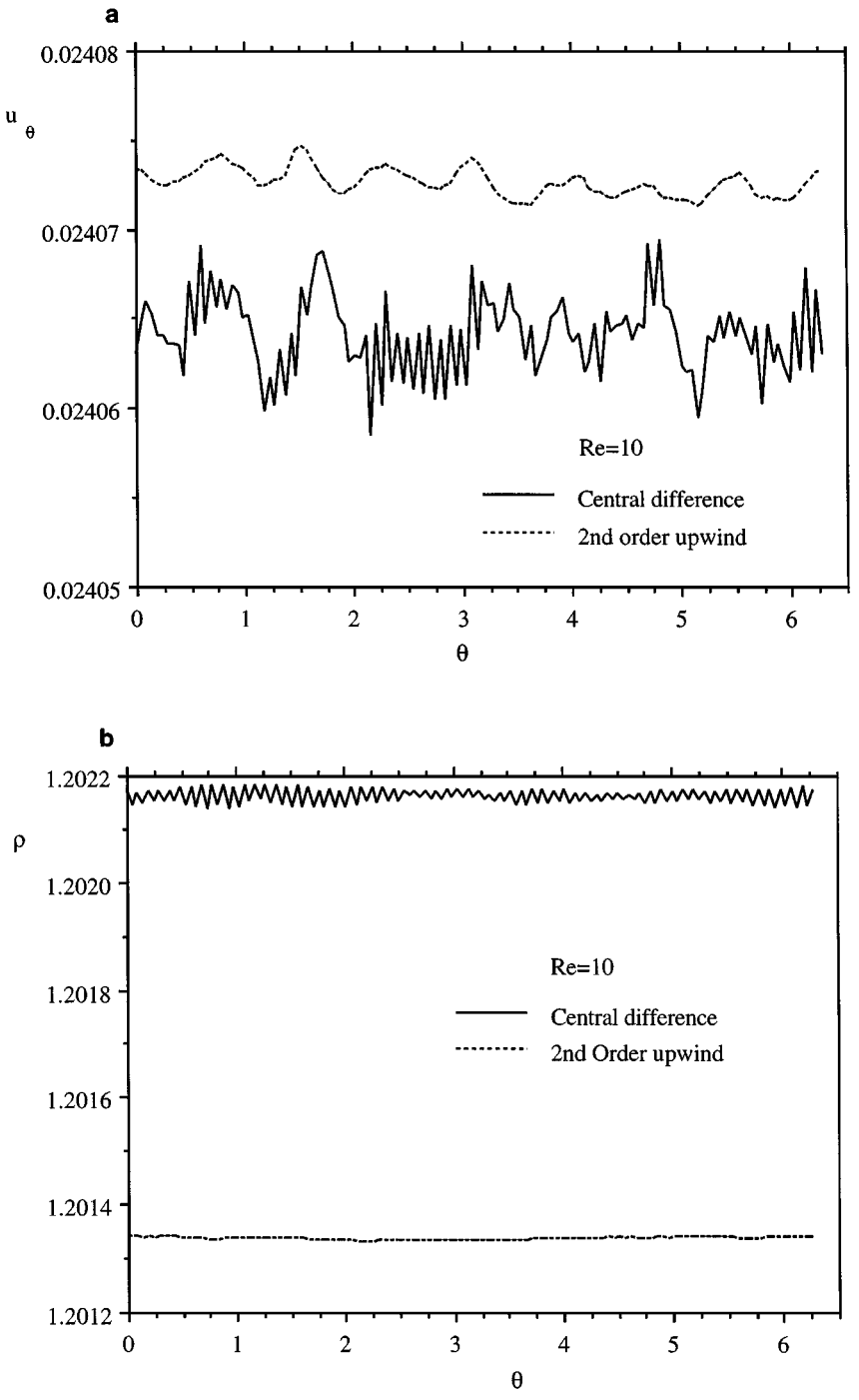

FIG. 4. Variations of steady state solutions in cylindrical Couette flow. (a) Tangential velocity along θ at $y = 0.9084$; (b) density along θ at $y = 0.9084$; (c) density along the r-direction. The reference density is taken from $r = r_1$. For the central difference case, the reference density is taken from the average at $r = r_1$ and the next grid in the flow field. Mixed denotes the use of $(\partial f_i^n/\partial\theta)|_{centr}$ and $(\partial f_i^n/\partial\eta)|_{2up}$ in Eq. (15).

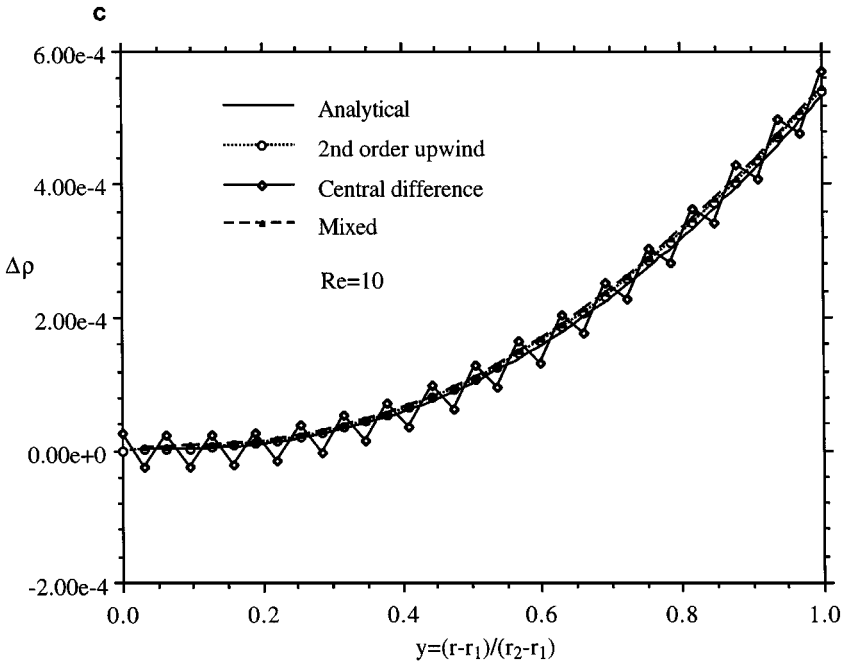

FIG. 4—*Continued*

with the exact solution, it is instructive to see if changing $(\partial f_i^n/\partial\eta)|_{centr}$ to $(\partial f_i^n/\partial\eta)|_{2up}$ while keeping $\partial f_i^n/\partial\theta$ in the central difference form in Eq. (15) could eliminate the grid-scale oscillation in the r-direction. The result based on the mixed difference scheme for the advection term is also shown in Fig. 4(c). It is seen that it agrees well with the analytical solution. This example indicates that the advection terms in each direction may be separately approximated to achieve satisfactory results in using FDLBM. This feature will be explored further when solving the external flow over a circular cylinder.

3.3. *Steady Flow over a Flat Plate*

Flow over a flat plate of finite length, L, placed parallel to the free stream, is considered next (see Fig. 5). Because of the simplicity in the geometry, the standard LBGK approach, Eq. (4), can be used to obtain the solution to the flow field. It needs to be pointed out in the outset that since grid stretching can be applied in the FDLBM, flow over a flat plate in

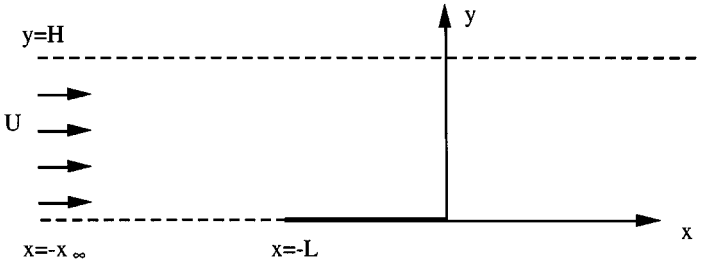

FIG. 5. Sketch for flow over a stack of flat plates.

an unbounded domain can be handled. In order to compare the results using the standard LBGK approach, a periodic condition is imposed in the y-direction at $y = \pm H$ to reduce the computational effort in using LBGK. In order to assess the performance of FDLBM and LBGK procedures meaningfully, all computations are made on a grid system consisting of 100 intervals in the x-direction and 50 in the y-direction.

In the FDLBM for this flow, the following coordinate transformation from (x, y) to (ξ, η) in which $0 \le \xi \le 1$, $0 \le \eta \le 1$ is applied:

$$z = -1 + \left(1 - \frac{z_\infty}{L}\right)\frac{e^{\beta(\xi_0 - \xi)} - 1}{e^{\beta\xi_0} - 1}, \qquad 0 \le \xi \le \xi_0 \tag{22a}$$

$$z = -c_\xi \tan^{-1}\left[\tan\left(\frac{1}{c_\xi}\right)\frac{0.5 - \xi}{0.5 - \xi_0}\right], \qquad \xi_0 \le \xi \le 0.5. \tag{22b}$$

This transforms $0 \le \xi \le 0.5$ into $-z_\infty \le z \le 0$. A symmetry condition is then utilized for $z > 0$. The relation between x and ξ is established through

$$x/L = (z - 1)/2. \tag{23}$$

The parameter z_∞ determines the extent of the domain in the x-direction. After z_∞, ξ_0, and β are specified as input, c_ξ is determined by requiring the derivative $dz/d\xi$ to be continuous at $\xi = \xi_0$. In the y-direction, the following is used

$$\frac{y}{L} = \frac{H}{L}\frac{e^{c_\eta \eta} - 1}{e^{c_\eta} - 1}. \tag{24}$$

The boundary conditions are described as follows. On the symmetry line at $y = 0$ $(jy = 2)$, a certain symmetry condition holds for the distribution functions f_i's so that the f_i's at $y = -\Delta y$ $(jy = 1)$ are obtained as

$$\begin{aligned}
&f_0(jx, 1) = f_0(jx, 3), \quad && f_1(jx, 1) = f_1(jx, 3), \quad && f_2(jx, 1) = f_8(jx, 3)\\
&f_3(jx, 1) = f_7(jx, 3), \quad && f_4(jx, 1) = f_6(jx, 3), \quad && f_5(jx, 1) = f_5(jx, 3)\\
&f_6(jx, 1) = f_4(jx, 3), \quad && f_7(jx, 1) = f_3(jx, 3), \quad && f_8(jx, 1) = f_2(jx, 3)
\end{aligned} \tag{25}$$

for $x > 0$ and $x < -L$. Similar symmetry conditions hold also at $y = H$. At $y = 0$, $-L \le x \le 0$, the extrapolation condition, Eq. (17), is applied while the no-slip condition for the velocity is imposed. At the inlet, $jx = 2$, the uniform velocity distribution,

$$u(jx = 2, iy) = U \qquad \text{and} \qquad v(jx = 2, jy) = 0, \tag{26}$$

is imposed. The distribution functions $f_i(jx = 1, jy)$ are set to equal $f_i(jx = 2, jy)$

$$f_i(jx = 1, jy) = f_i(jx = 2, jy) \tag{27}$$

because of the uniformity of the flow. At the exit, $jx = Nx - 1$, a zeroth order extrapolation is used, i.e.,

$$u(Nx - 1, jy) = u(Nx - 2, jy) \qquad \text{and} \qquad v(Nx - 1, jy) = 0. \tag{28}$$

The distribution function at $jx = Nx$ is obtained using linear extrapolation

$$f_i(Nx, jy) = 2 f_i(Nx - 1, jy) - f_i(Nx - 2, jy). \tag{29}$$

The conditions given by (28)–(29) allow the wake velocity to be developed.

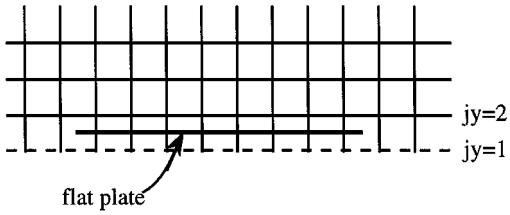

FIG. 6. Lattice arrangement in LBGK near the plate.

Using the same transformed coordinates, the vorticity-stream function based NS equations [15] are also solved and the results provide the basis for comparison with LBM based solutions. The computational domain is $H/L = 5$, $z_\infty/L = 5$ with $L = 10$ lattice units. The non-uniform grids are generated using the following parameters: $\xi_0 = 0.32$, $c_\xi = 1$, which gives $\beta = 12.17473$ in Eq. (22a), and $c_\xi = 4$ in Eq. (24). In both FDLBM and $\omega - \psi$ formulation, 100 intervals in the ξ-direction and 50 intervals in the η-direction are used. This gives a total of 36 intervals on the surface of the plate. For $Re = 10$, $\tau = 0.25$ is used so that $\nu = \tau/3 = 0.08333$ and $U = 0.08333$. For $Re = 100$, $\tau = 0.025$ and $\nu = 0.008333$. In both cases, the time step is $\Delta t = 0.025$ which is mainly dictated by the spatial resolution.

The LBGK based solution is obtained using the standard streaming-collision procedure with $\Delta x = \Delta y = \Delta t = 1$. For $Re = 10$, $\tau = 0.75$ is used so that $\nu = (2\tau - 1)/6 = 0.08333$ and $U = 0.08333$ for $L = 10$. For $Re = 100$, $\tau = 0.55$ so that $\nu = 0.008333$ and $U = 0.08333$. The solid wall is placed halfway between lattices (grids) indicated by $jy = 1$ and $jy = 2$, as shown in Fig. 6. A standard bounce-back condition for the f_i's [11, 12] on the plate is implemented. Away from the plate, the symmetry conditions are enforced in a manner similar to Eq. (25) except that $jy = 3$ is replaced by $jy = 2$ in a form such as $f_7(jx, 1) = f_3(jx, 2)$. One hundred intervals in the x-direction and 50 intervals in the y-direction are used in LBGK solution. Since $L = 10$, there are only 10 lattices (grids) on the plate. The inlet and exit of the computational domain are at $x/L = -6$ and 4 so that $\Delta x = 1$ with 100 intervals in the x-direction.

Figure 7(a) compares the centerline velocities from three solutions based on $\omega - \psi$ formulation, FDLBM, and LBGK at $Re = 10$. The centerline velocity in LBGK is obtained using extrapolation from $jy = 2$ and $jy = 3$ together with the symmetry condition. Overall, three solutions agree very well in both upstream and downstream. Because the grid strecthing is applied near the leading edge and the trailing edge in FDLBM while a uniform grid is used in LBGK, FDLBM based solution agrees with the $\omega - \psi$ based solution better than the LBGK solution near the leading edge, as shown in the inset of Fig. 7(a). Figure 7(b) compares the velocity profiles in the middle of the plate, $u(y, x/L = -0.5)$. Since the singularity has little effect at $x/L = 0.5$, all three solutions agree well in regions near the wall and near the symmetry line. Figure 7(c) compares the wall vorticity $(L/U)(\partial u/\partial y)$ along the plate from these three solutions. It is seen that LBGK solution agrees well with the $\omega - \psi$ based solution on almost all of the grids. Near the leading and trailing edges, the resolution in LBGK is insufficient to observe a rapid rise in the vorticity. The FDLBM based solution for the wall vorticity exhibits an oscillatory behavior near the leading and trailing edges. A closer examination of the flow field reveals that the oscillation in velocity, hence vorticity, is associated with a rapid variation in density ρ near the edges. Figure 8 shows the variation of ρ in the x-direction near the plate for both $Re = 10$ and $Re = 100$. In the near incompressible flow limit, the density variation is viewed as the pressure variation. The

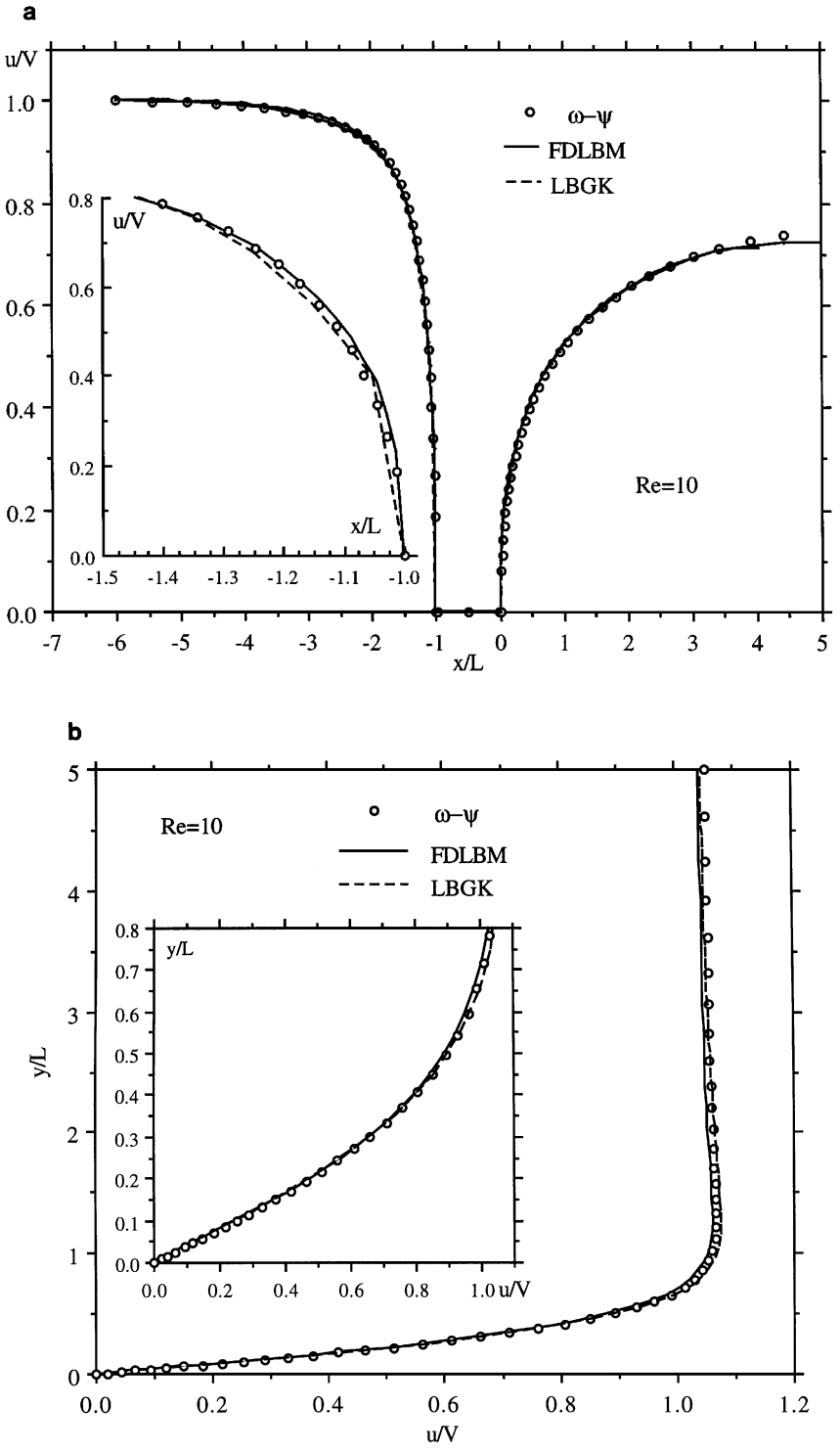

FIG. 7. (a) Centerline wake velocity at $Re = 10$ from three solutions. (b) Velocity profile in the middle of the plate at $Re = 10$. (c) Surface vorticity on the plate at $Re = 10$.

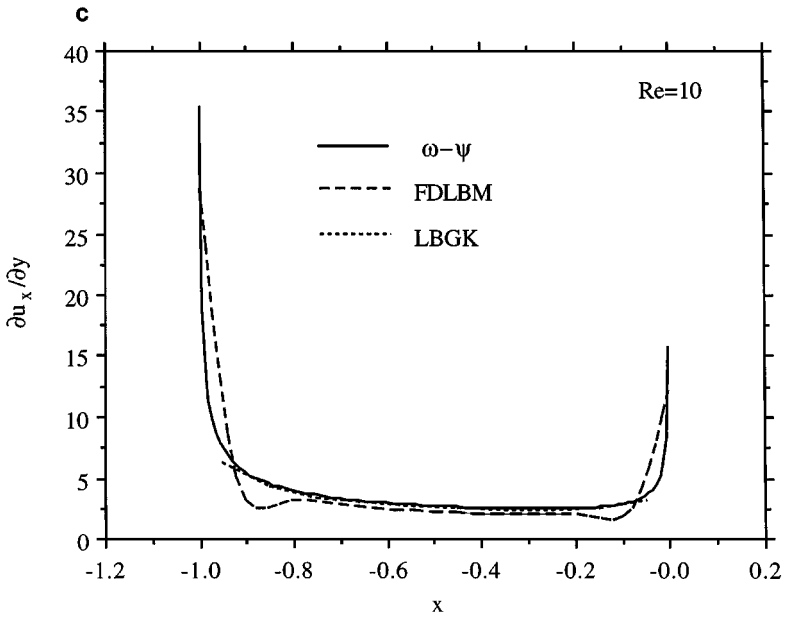

FIG. 7—*Continued*

oscillation in p along the x-direction results from the singularity in the boundary condition near the edges. In LBGK, the plate is located halfway between the lattices (see Fig. 6) so that the density at $jy = 2$ is much less singular as the grid is off the plate. In the $\omega - \psi$ formulation, the pressure is decoupled from the primary variable ω while the velocity is evaluated by taking derivatives of ψ. The fact that the LBGK has a better agreement for

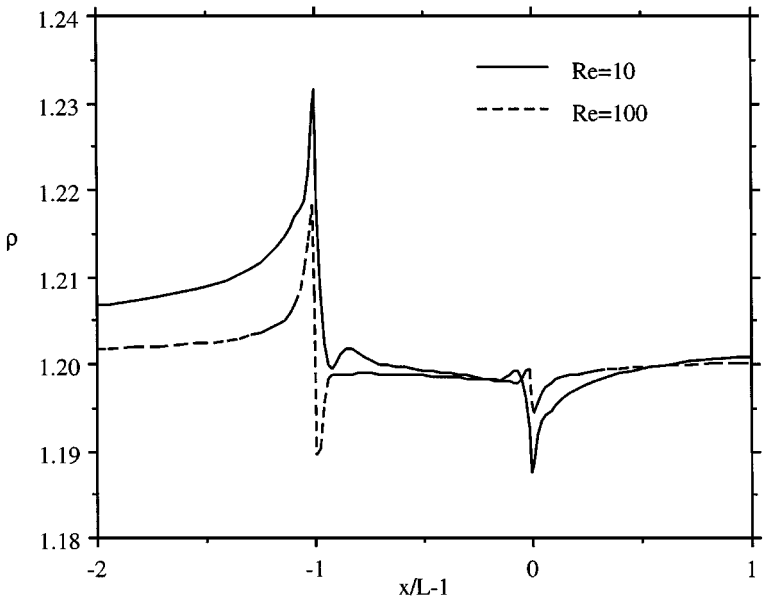

FIG. 8. Density variations from FDLBM on the symmetry axis and plate at $Re = 10$ and 100.

wall vorticity with that based on the $\omega - \psi$ formulation is thus attributed to the way the grids are arranged.

Figure 9(a) compares the centerline velocities based on three solutions at $Re = 100$. All solutions are based on 100×50 grids. Due to insufficient resolution near the plate in LBGK, a noticeable difference in $u(x)$ is observed between LBGK based and $\omega - \psi$ based solutions in both upstream and downstream regions. Figure 9(b) shows velocity profiles $u(y)$ near the plate ($Y/L < 0.5$) at $x/L = -0.95, -0.5$, and -0.05 from these three solutions. Reasonable agreement is observed between FDLBM and $\omega - \psi$ based solutions. Again, due to insufficient resolution ($\Delta y/L = 0.1$) at higher Reynolds number, the velocity profile near the leading edge in LBGK exhibits unphysical oscillation. If the standard LBGK procedure is to be used for flow problems with such kind of singularities at higher Reynolds number, much better resolution should be used.

3.4. *Steady Flow over a Circular Cylinder*

Flow over a circular cylinder (Fig. 10) is most conveniently carried out in polar coordinates. In LBGK procedure with square lattice, the cylindrical surface is only approximately described. Due to the use of the uniform grid, it is impractical to compute an unbounded flow over the cylinder. Hence comparisons for the flow field will be made between the $\omega - \psi$ based solutions and FDLBM based solution.

In applying FDLBM for the flow field, the following coordinate stretching similar to Eq. (19) is used,

$$r = r_1 + (r_\infty - r_1)\left\{1 - \frac{1}{\beta}\tan^{-1}[(1-\eta)\tan(\beta)]\right\}. \tag{30}$$

The cylinder radius $r_1 = 10$ is used. To examine the effect of the domain size on the solution, two values of the ratio r_∞/r_1 (100 and 1000) are used. In the $\omega - \psi$ formulation, the same coordinate stretching is implemented with $r_1 = 1$. Uniform grids in the θ-direction are adopted in both solution procedures. In the $\omega - \psi$ formulation using finite difference discretization, the second order upwind scheme is applied in both the r- and θ-directions. In the FDLBM the second order upwind is applied to the r-direction only, since the central difference for the advection term in the θ-direction does not result in any unphysical oscillation.

Figure 11(a) compares the dimensionless surface vorticity on the cylinder between the $\omega - \psi$ based solution and FDLBM based solution at $Re = 10$. In both computations, $r_\infty/r_1 = 100$, $\beta^{-1} = 0.65$, with 128 and 64 intervals in the r- and θ-directions, respectively. In FDLBM, $\tau = 0.4$, $U = 0.0667$. Since the vorticity is a near field quantity, it is seen that agreement between the two solutions is very good in the near field on the same computational domain with the same grid resolutions. Figure 11(b) compares the wall vorticity of the present solution with that given by Fornberg [7] for steady flow at $Re = 100$. The present FDLBM solution used 256 and 128 intervals in the r- and θ-directions, respectively, for $Re = 100$ with $\tau = 0.04$, $U = 0.0667$. The steady state solution is obtained without vortex shedding since no artificial asymmetry in the initial condition was introduced. Again, the agreement is reasonable.

Figure 12 compares the profiles of the x-component velocity at $x = 0$ at $Re = 10$. Two grid systems are used in FDLBM: (i) $r_\infty/r_1 = 100$ and $\beta^{-1} = 0.65$; (ii) $r_\infty/r_1 = 1000$ and $\beta^{-1} = 0.645$ with (128, 64) grid intervals in (r, θ). In the $\omega - \psi$ formulation, three sets of solutions are obtained: (i) $r_\infty/r_1 = 100$, $\beta^{-1} = 0.65$ with (128, 64) intervals; (ii) $r_\infty/r_1 = 1000$

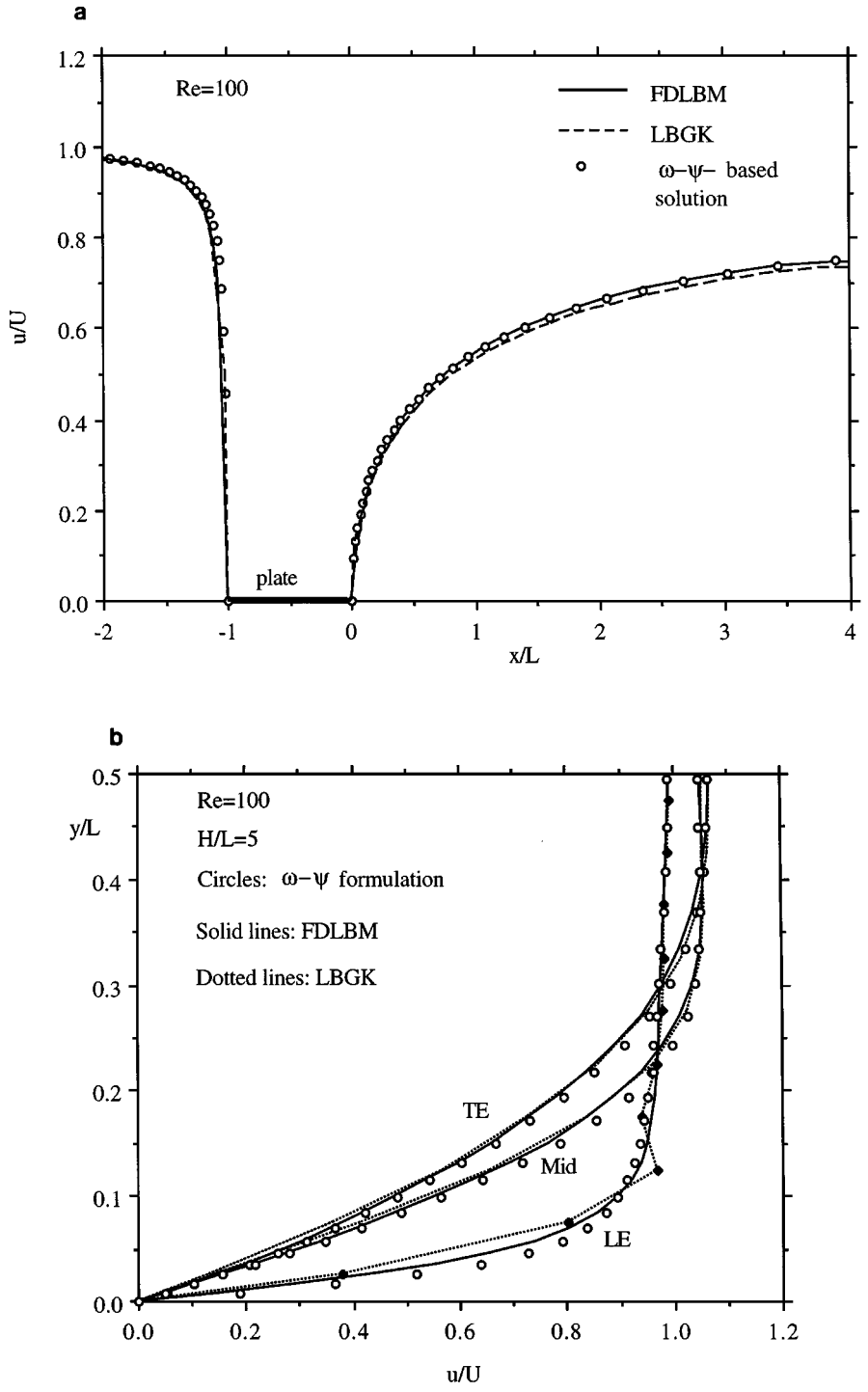

FIG. 9. (a) Comparison of the centerline wake velocity from three solutions. (b) Comparison of the velocity profiles on the plate based on three solutions at $Re = 100$.

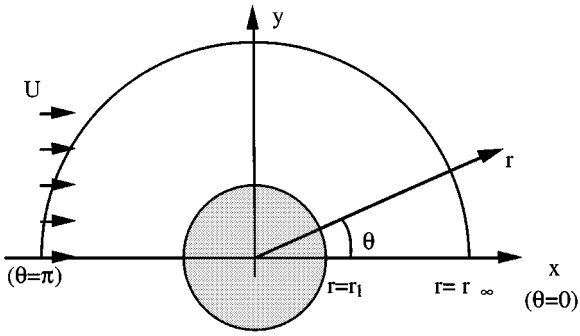

FIG. 10. Sketch of flow over a circular cylinder.

and $\beta^{-1} = 0.645$ with (128, 64) intervals; (iii) $r_\infty/r_1 = 1000$ and $\beta^{-1} = 0.645$ with (128, 128) intervals. The u-velocity profiles based on the $\omega - \psi$ formulation obtained with $r_\infty/r_1 = 1000$ on 128×128 grids are virtually identical to that on the 128×64 grid for $y/r - 1 \leq 10$; so only one is presented. It is observed that FDLBM solution on either grid agrees very well with the $\omega - \psi$ based solution obtained on 128×128 grids and $r_\infty/r_1 = 1000$.

For flows in an unbounded domain, it is important to examine the behavior and accuracy of FDLBM solution in the far field. Figure 13(a) shows the wake centerline velocity obtained from two solutions on various grids in the region of $r/r_1 < 100$. For the far field, the best resolution is the $\omega - \psi$ based solution with $r_\infty/r_1 = 1000$ on a 128×128 grid. This grid system extends 1000 radii downstream and has a better resolution in the θ-direction so that the narrow wake (whose width scales with $(x\nu/U)^{1/2}$ [17]) is better resolved than other grid systems used here. In general, if the wake is not sufficiently resolved, the vorticity in the wake decays more rapidly (in most cases exponentially) than algebraically in the x-direction so that the velocity recovery to the free stream value is faster. The solutions based on $r_\infty/r_1 = 100$ are obviously affected by the boundary condition near $r = r_\infty$. Of the two solutions obtained on $r_\infty/r_1 = 1000$ and 128×64 grids, the FDLBM-based solution appears to be better than the $\omega - \psi$ based solution on the same grid. Figure 13(b) shows the decay of wake velocity in the form of $1 - u/U$ in $x/r_1 - 1 \leq 1000$. The decay should follow an $x^{-1/2}$ asymptotic behavior. It is clear that the FDLBM-based solution on $r_\infty/r_1 = 1000$ and 128×64 grids has a slightly larger region exhibiting this asymptotic behavior than the $\omega - \psi$-based solution on the same grid system.

The length of the separation bubble (L) and the separation angles θ are also obtained using FDLBM on the same grid (with 128 and 64 intervals in the r- and θ-directions). They are $(L/r_1, \theta) = (0.498, 30.0^\circ)$, $(1.804, 42.1^\circ)$, and $(4.38, 50.12^\circ)$ for $Re = 10$, 20, and 40. The present results compare reasonably well with those reported by He and Doolen [10] using interpolation supplemented LBM with finer grids: $(L/r_1, \theta) = (0.474, 26.89^\circ)$, $(1.842, 42.96^\circ)$, and $(4.49, 52.84^\circ)$ for $Re = 10$, 20, and 40.

Direct comparison of the computational efficiency between FDLBM and the conventional CFD method, such as finite difference, requires careful implementation of both methods on the same physical problems on the same machine. Some related information of the LBM and the NS solvers on parallel computation can be found in Maier *et al.* [14] and in Shyy *et al.* [19], respectively. However, many programming and unreported factors make a direct comparison between these approaches difficult. More work will be required in this regard. Based on the available information, it appears that the present approach is competitive to similar approaches. For example, He and Doolen [10] reported that for $Re = 10$ and 20, the

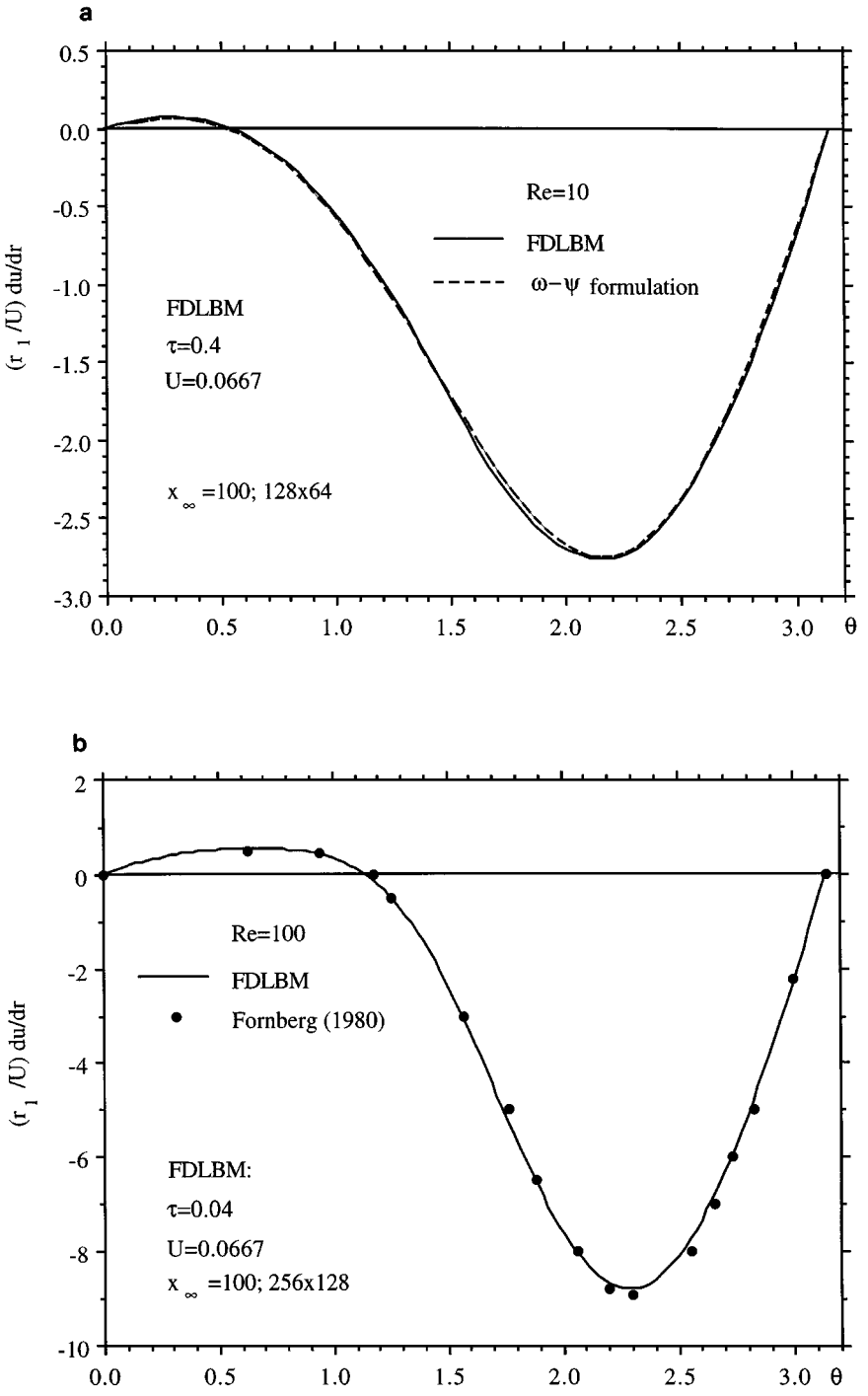

FIG. 11. Comparison of the surface vorticity on the cylinder. (a) $Re = 10$; (b) $Re = 100$.

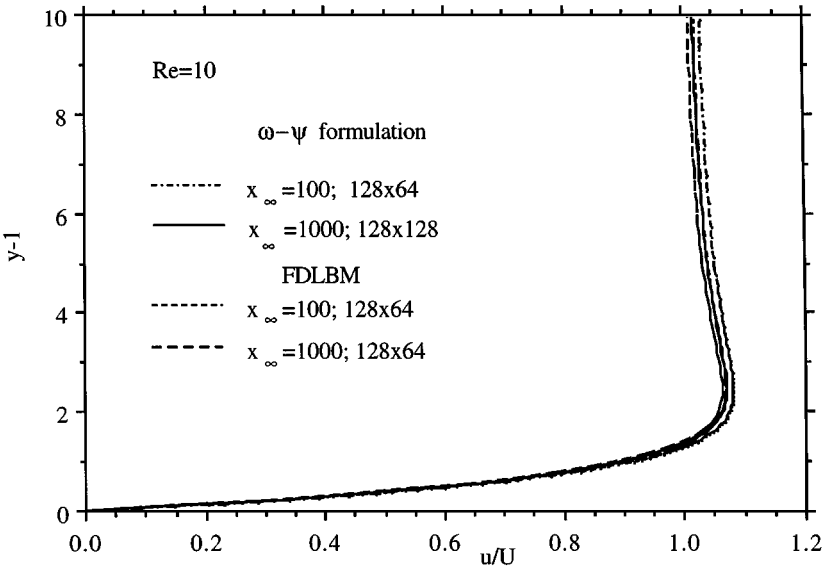

FIG. 12. Comparison of the x-component velocity at $x = 0$ between two solutions on various grids for flow over a cylinder.

time step used was 0.0025 times of r_1/U ($r_1 = 40$ lattice unit and $U = 0.1$). In our test case using $U = 0.1$, the time step was 0.002 times of r_1/U and computations were stable. On a DEC alpha Station with a single processor and a clock speed of 256 MHz, each time step takes about 0.058 s on 65×129 grid points. In the interpolation supplemented LBM, the extra work is in the second order interpolation in comparison with the classical LBGK. In the present case, the extra work is in the evaluation of the advective term. The amount of work is comparable between the two approaches [13].

4. SUMMARY AND CONCLUSIONS

The finite difference-based lattice Boltzmann method (FDLBM) suggested by Cao *et al.* [3] is extended to curvilinear coordinates with non-uniform grids. The geometry of curved boundaries is preserved in body-fitted coordinates. The non-uniform grids allow the use of a much larger computational domain to minimize the effect of the outflow boundary condition. A single step method, instead of the predictor-corrector procedure as used in Cao *et al.* [3], is implemented. The relaxation term in the transport equation for the distribution function f_i's is treated semi-implicitly to improve the stability while the procedure for the evaluation of f_i's remains explicit. Detailed examinations of various flows (impulsively started cylindrical Couette flow, steady state cylindrical Couette flow, steady flow over flat plates, and steady flow over a circular cylinder) are carried out.

The extrapolation based boundary condition for the distribution function f_i's on a solid wall [5] is extended to curvilinear coordinates. Results based on this treatment agree well with either analytical solutions or results based on other numerical methods. The use of central difference discretization for the advection terms in the transport equations for f_i's typically results in wiggles on the grid scale in the solution which can lead to numerical instability. The second order upwind difference for the advection term should then be used to eliminate these wiggles. For the first time, it is demonstrated that the Lattice Boltzmann

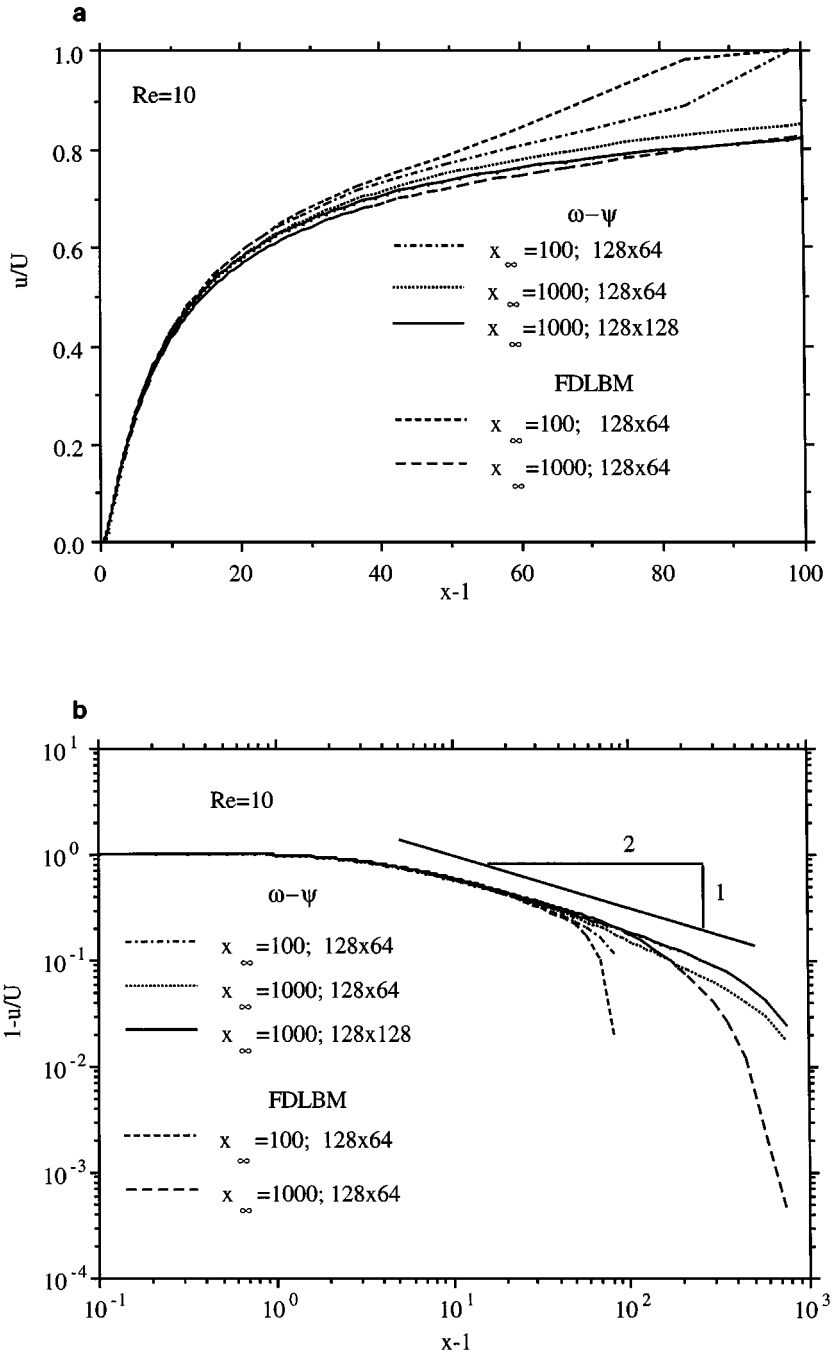

FIG. 13. (a) Comparison of the wake centerline velocity in $x/r_1 \leq 100$ between two solutions on various grids. (b) Decay of the wake centerline velocity based on two solutions obtained with various grids.

method can capture the far wake flow field accurately by using non-uniform grids. Favorable results obtained using FDLBM in curvilinear coordinates indicate that the method is potentially capable of solving finite Reynolds number flow problems in complex geometries.

ACKNOWLEDGMENTS

R. Mei acknowledges partial support of the Alcoa Foundation, the Engineering Research Center (ERC) for Particle Science and Technology at the University of Florida, the National Science Foundation (EEC-9402989), and industrial partners of the ERC. W. Shyy acknowledges partial support of the Alcoa Foundation, AFOSR, and Eglin AFB.

REFERENCES

1. T. Abe, Derivation of the lattice Boltzmann method by means of the discrete ordinate method for the Boltzmann equation, *J. Comput. Phys.* **131**, 241 (1997).
2. P. L. Bhatnagar, E. P. Gross, and M. Krook. A model for collision processes in gases. I. Small amplitude processes in charged and neutral one-component system, *Phys. Rev.* **94**, 511 (1954).
3. N. Z. Cao, S. Chen, S. Jin, and D. Martinez, Physical symmetry and lattice symmetry in lattice Boltzmann method, *Phys. Rev. E* **55**, R21 (1997).
4. S. Chen and G. D. Doolen, Lattice Boltzmann method for fluid flows, *Ann. Rev. Fluid Mech.* **30**, 329 (1998).
5. S. Chen, D. Martinez, and R. Mei, On boundary conditions in lattice Boltzmann method, *Phys. Fluids* **8**(9), 2527 (1996).
6. H. Chen, S. Chen, and W. H. Matthaeus, Recovery of the Navier–Stokes equations using a lattice-gas Boltzmann method, *Phys. Rev. A* **45**, R5339 (1992).
7. B. Fornberg, A numerical study of steady viscous flow past a circular cylinder, *J. Fluid Mech.* **98**, 819 (1980).
8. X. He and L. S. Luo, A *priori* derivation of the lattice Boltzmann equation, *Phys. Rev. E* **55**(6), R6333 (1997).
9. X. He, L. S. Luo, and M. Dembo. Some progress in lattice Boltzmann method. Part I. nonuniform mesh grids, *J. Comput. Phys.* **129**, 357 (1996).
10. X. He and G. Doolen, Lattice Boltzmann method on curvilinear coordinates system: Flow around a circular cylinder, *J. Comput. Phys.* **134**, 306 (1997).
11. A. J. C. Ladd, Numerical simulation of particular suspensions via a discretized Boltzmann equation. Part 1. Theoretical foundation, *J. Fluid Mech.* **271**, 285 (1994).
12. A. J. C. Ladd, Numerical simulation of particular suspensions via a discretized Boltzmann equation. Part 2. numerical results, *J. Fluid Mech.* **271**, 311 (1994).
13. L. S. Luo, private communication, 1998.
14. R. S. Maier, D. M. Kroll, Y. E. Kutsovsky, H. T. Davis, and R. S. Bernard, Simulation of flow through bead packs using the lattice Boltzmann method, *Phys. Fluids* **10**(1), 60 (1998).
15. R. Mei and A. Plotkin, A finite difference scheme for the solution of the steady Navier–Stokes equation, *Comput. & Fluids* **14**(3), 239 (1986).
16. D. R. Noble, S. Chen, J. G. Georgiadis, and R. O. Buckius, A consistent hydrodynamic boundary condition for the lattice Boltzmann method, *Phys. Fluid* **7**, 203 (1995).
17. H. Schlichting, *Boundary Layer Theory* (McGraw–Hill, New York, 1979), 7th ed.
18. W. Shyy, *Computational Modeling for Fluid Flow and Interfacial Transport* (Elsevier, Amsterdam, 1994, corrected printing, 1997).
19. W. Shyy, S. T. Thakar, H. Ouyang, J. Liu, and E. Blosch, *Computational Techniques for Complex Transport Phenomena* (Cambridge Univ. Press, New York, 1997).
20. S. Succi, Lattice Boltzmann equation: Failure or success? *Phys. A* **240**, 221 (1997).